Inorg. Chem. **2006**, *45*, 10743–10749

Spin Dimer Analysis of the Magnetic Structures of $Ba_3Cr_2O_8$, $Ba_3Mn_2O_8$, Na_4FeO_4, and Ba_2CoO_4 with a Three-Dimensional Network of Isolated MO_4 (M = Cr, Mn, Fe, Co) Tetrahedra

Hyun-Joo Koo*

Department of Chemistry and Research Institute of Basic Science, Kyung Hee University, Seoul 130-701, South Korea

Kwang-Soon Lee† and Myung-Hwan Whangbo*

Department of Chemistry, North Carolina State University, Raleigh, North Carolina 27695-8204

Received September 19, 2006

The spin exchange interactions of the magnetic oxides $Ba_3Cr_2O_8$, $Ba_3Mn_2O_8$, Na_4FeO_4, and Ba_2CoO_4 with a three-dimensional network of isolated MO_4 (M = Cr, Mn, Fe, Co) tetrahedra were examined by performing spin dimer analysis on the basis of tight-binding electronic structure calculations. Although the shortest O···O distances between adjacent MO_4 tetrahedra are longer than the van der Waals distance, our analysis shows that the super-superexchange interactions between adjacent MO_4 tetrahedra are substantial and determine the magnetic structures of these oxides. In agreement with experiment, our analysis predicts a weakly interacting isolated AFM dimer model for both $Ba_3Cr_2O_8$ and $Ba_3Mn_2O_8$, the (0.0, 0.5, 0.0) magnetic superstructure for Na_4FeO_4, the (0.5, 0.0, 0.5) magnetic superstructure for Ba_2CoO_4, and the presence of magnetic frustration in Ba_2CoO_4. The comparison of the intra- and interdimer spin exchange interactions of $Ba_3Cr_2O_8$ and $Ba_3Mn_2O_8$ indicates that orbital ordering should be present in $Ba_3Cr_2O_8$.

1. Introduction

A three-dimensional (3D) network of isolated MO_4 tetrahedra containing transition metal ions M^{n+} (n = 4, 5) in high oxidation state is present in a number of magnetic oxides, which include β-Ba_2VO_4,[1] Sr_2VO_4,[2] A_2CrO_4 (A = Sr, Ba),[3] $Ba_3Cr_2O_8$,[4] $Ba_3Mn_2O_8$,[5] Ba_2FeO_4,[6] Na_4FeO_4,[7] and Ba_2CoO_4.[8] The transition metal ions V^{4+} (d^1), Cr^{5+} (d^1), Mn^{5+} (d^2), Fe^{4+} (d^4), and Co^{4+} (d^5) present in those compounds possess unpaired spins responsible for their magnetic properties, and the Fe^{4+} (d^4) and Co^{4+} (d^5) ions are in high-spin state.[7,8a,b] The MO_4 tetrahedra are well-separated from each other by Ba^{2+}, Sr^{2+}, or Na^+ ions, so that the shortest O···O distances between adjacent MO_4 tetrahedra are longer than the van der Waals distance (i.e., 2.80 Å). Thus, one might speculate that the spin exchange interactions between adjacent spin sites are negligible, so these magnetic oxides are paramagnetic. However, their magnetic properties show the presence of substantial antiferromagnetic (AFM) spin exchange interactions between adjacent MO_4 tetrahedra. For example, both $Ba_3Cr_2O_8$ and $Ba_3Mn_2O_8$ have a spin gap and are described by a weakly interacting AFM dimer model.[4,5a−c] Na_4FeO_4 undergoes a 3D AFM ordering below the Néel temperature T_N = 16 K and has a magnetic superstructure (0.0, 0.5, 0.0) at 2 K[7a] (i.e., the magnetic cell is doubled

* To whom correspondence should be addressed. E-mail: hjkoo@khu.ac.kr (H.-J.K.); mike_whangbo@ncsu.edu (M.-H.W.).

† Permanent address: Department of Chemistry, The Catholic University of Korea, Bucheon, Gyeonggi-Do, South Korea 422-743.

(1) (a) Liu, G.; Greedan, J. E. *J. Solid State Chem.* **1993**, *103*, 228. (b) Feltz, A.; Schmalfuss, S. *Z. Chem.* **1975**, *15*, 323.
(2) Gong, W.; Greedan, J. E.; Liu, G.; Bjorgvinsson. *J. Solid State Chem.* **1991**, *94*, 213.
(3) (a) Guo, L.; Greedan, J. E.; Gong, W. *J. Solid State Chem.* **1993**, *105*, 78. (b) Wilhelmi, K. A. *Ark. Kemi* **1966**, *26*, 157.
(4) Nakajima, T.; Mitamura, H.; Ueda, Y. *J. Phys. Soc. Jpn.* **2006**, *75*, 54706. (b)
(5) (a) Tsujii, H.; Andraka, B.; Uchida, M.; Tanaka, H.; Takano, Y. *Phys. Rev. B* **2005**, *72*, 214434. (b) Uchida, M.; Tanaka, H.; Mitamura, H.; Ishikawa, F.; Goto, T. *Phys. Rev. B.* **2002**, *66*, 54429. (c) Uchida, M.; Tanaka, H.; Bartashevich, M. I.; Goto, T. *J. Phys. Soc. Jpn.* **2001**, *70*, 1790. (d) Weller, M. T.; Skinner, S. J. *Acta Crystallogr., Sect. C* **1999**, *55*, 154.
(6) Delattre, J. L.; Stacy, A. M.; Young, V. G., Jr.; Long, G. L.; Herman, R.; Grandjean, F. *Inorg. Chem.* **2002**, *41*, 2834.
(7) (a) Jeannot, C.; Malaman, B.; Gérardin, R.; Oulladiaf, B. *J. Solid State Chem.* **2002**, *165*, 266. (b) Weller, M. T.; Hector, A. L. *Angew. Chem., Int. Ed.* **2000**, *39*, 4162. (c) Scholder, R.; Bunsen, Hv.; Zeiss, W. *Z. Anorg. Allg. Chem.* **1956**, *283*, 330.
(8) (a) Boulahya, K.; Parras, M.; González-Calbet, J. M.; Amador, U.; Martínez, J. L.; Fernández-Díaz, M. T. *Chem. Mater.* **2006**, *18*, 3898. (b) Jin, R.; Sha, H.; Khalifah, P. G.; Sykora, R. E.; Sales, B. C.; Mandrus, D.; Zhang, J. *Phys. Rev. B.* **2006**, *73*, 174404. (c) Boulahya, K.; Parras, M.; Vegas, A.; Gonzalez-Calbet, J. M. *Solid State Sci.* **2000**, *2*, 57. (d) Candela, G. A.; Kahn, A. H.; Negas, T. *J. Solid State Chem.* **1973**, *7*, 360.

10.1021/ic061773c CCC: $33.50
Published on Web 12/02/2006

along the *b*-axis with respect to the crystallographic cell). Similarly, Ba_2CoO_4 undergoes a 3D AFM ordering below $T_N = 23$ K[8a,b] and has a magnetic superstructure (0.5, 0.0, 0.5) at 4 K (i.e., the magnetic cell is doubled along the *a*- and *c*-axes with respect to the crystallographic cell).[8a] So far, there has been no theoretical study aimed at understanding the various magnetic properties of those oxides with a 3D network of isolated MO_4 tetrahdra.

Magnetic interactions between unpaired spins include spin exchange and dipole interactions. Spin exchange interactions between adjacent spin sites occur through the overlap between the tails of their magnetic orbitals and hence are short-ranged,[9] while dipole interactions occur through space and are long-ranged. In general, a spin exchange interaction between adjacent spins can be stronger than a dipole interaction between them by a factor of 1000 or greater.[10] Therefore, to understand the magnetic properties of the oxides made up of isolated MO_4 tetrahedra, it is necessary to examine the spin exchange interactions between adjacent MO_4 tetrahedra, which should take place through the M−O···O−M super-superexchange paths.[9] We note that the magnetic sulfides $BaLn_2MnS_5$ (Ln = La, Ce, Pr) have a 3D network of isolated MnS_4 tetrahedra with high-spin Mn^{2+} ions and undergo a 3D AFM ordering at a reasonably high temperature (i.e., $T_N = 58.5$, 62.0, and 64.5 K for Ln = La, Ce, and Pr, respectively),[11] although the shortest S···S distances between adjacent MnS_4 tetrahedra are longer than the van der Waals distance (3.6 Å). This finding is well explained in terms of their super-superexchange interactions between adjacent MnS_4 tetrahedra, which take place through the Mn−S···S−Mn paths, as shown by our spin dimer analysis[12] on the basis of the extended Hückel tight binding (EHTB) calculations.[9,13] By employing this spin dimer analysis, we probe in this work the spin exchange interactions of $Ba_3Cr_2O_8$, $Ba_3Mn_2O_8$, Na_4FeO_4, and Ba_2CoO_4 to account for their magnetic properties.

2. Spin Dimer Analysis

Magnetic properties of a solid are commonly described by a Heisenberg spin Hamiltonian written as a sum of pairwise isotropic spin exchange interactions, $J_{ij}\hat{S}_i \cdot \hat{S}_j$, where $\hat{S}_i$ and $\hat{S}_j$ are the spin operators at the spin sites *i* and *j*, respectively, and J_{ij} is the spin exchange parameter. This Hamiltonian expresses the energy differences between different magnetic states of a magnetic solid in terms of a chosen set of spin exchange parameters J_{ij}. Within the framework of first principles electronic structure theory, the spin exchange parameters of a magnetic solid are estimated either by calculating the electronic structures for the high- and low-spin states of various spin dimers (i.e., structural units consisting of two spin sites) of the solid[14] or by calculating the electronic band structures for various ordered spin states of the solid.[15] The energy differences between different electronic states are then mapped onto the corresponding energy differences given by the spin Hamiltonian employed.[16] In either explaining trends in spin exchange interactions of magnetic solids or testing the validity of a set of spin exchange parameters chosen to form a spin Hamiltonian, it is often sufficient to estimate the relative magnitudes of the spin exchange parameters.[9] In general, a spin exchange parameter *J* is written as $J = J_F + J_{AF}$.[17] The ferromagnetic term J_F (>0) is a small positive number, so that the spin exchange becomes ferromagnetic (i.e., $J > 0$) only when the AFM term J_{AF} (<0) is negligibly small in magnitude. Thus, AFM spin exchange interactions (i.e., $J < 0$) can be discussed by focusing on the AFM terms J_{AF}.[9] In spin dimer analysis based on EHTB calculations, the strength of an AFM interaction between two spin sites is estimated by considering the AFM spin exchange parameter J_{AF},[9]

$$J_{AF} \approx -\frac{<(\Delta e)^2>}{U_{eff}} \tag{1}$$

where U_{eff} is the effective on-site repulsion that is essentially a constant for a given compound. The $<(\Delta e)^2>$ term is calculated by performing EHTB electronic structure calculations for a spin dimer, which is given by two tetrahedra $(MO_4)\cdots(MO_4)$ for the magnetic oxides $Ba_3Cr_2O_8$, $Ba_3Mn_2O_8$, Na_4FeO_4, and Ba_2CoO_4.

The d-block levels of an MO_4 tetrahedron are split into the e_g and t_{2g} levels. The Cr^{5+} (d^1), Mn^{5+} (d^2), Fe^{4+} (d^4), and Co^{4+} (d^5) ions have the electronic configurations $(e_g)^1$, $(e_g)^2$, $(e_g)^2(t_{2g})^2$, and $(e_g)^2(t_{2g})^3$, respectively. For simplicity, we use the orbitals ϕ_1 and ϕ_2 for the two representing the doubly degenerate e_g level and ϕ_3, ϕ_4, and ϕ_5 for the three orbitals representing the triply degenerate t_{2g} level. In cases when all the sublevels of the e_g and t_{2g} levels are each singly occupied, the $<(\Delta e)^2>$ term is approximated by[9,12]

$$Mn^{5+}\ (d^2): \quad <(\Delta e)^2> \approx \frac{1}{2^2}\sum_{\mu=1}^{2}(\Delta e_{\mu\mu})^2 \tag{2}$$

$$Co^{4+}\ (d^5): \quad <(\Delta e)^2> \approx \frac{1}{5^2}\sum_{\mu=1}^{5}(\Delta e_{\mu\mu})^2 \tag{3}$$

(9) For recent reviews, see the following: (a) Whangbo, M.-H.; Koo, H. J.; Dai, D. *J. Solid State Chem.* **2003**, *176*, 417. (b) Whangbo, M.-H.; Dai, D.; Koo, H.-J. *Solid State Sci.* **2005**, *7*, 827.

(10) Ashcroft, N. W.; Mermin, N. D. *Solid State Physics*; Holt, Rinehart and Winston: Philadelphia, PA, 1976, pp 673−674.

(11) (a) Masuda, H.; Fujino, T.; Sato, N.; Yamada, K. *J. Solid State Chem.* **1999**, *146*, 336. (b) Wakeshima, M.; Hinatsu, Y. *J. Solid State Chem.* **2000**, *153*, 330. (c) Wakeshima, M.; Hinatsu, Y.; Oikawa, K.; Shimojo, Y.; Morii, Y. *J. Mater. Chem.* **2000**, *10*, 2183.

(12) Koo, H.-J.; Whangbo, M.-H.; Lee, K.-S. *J. Solid State Chem.* **2002**, *169*, 143.

(13) Hoffmann, R. *J. Chem. Phys.* **1963**, *39*, 1397.

(14) (a) Illas, F.; Moreira, I. de P. R.; de Graaf, C.; Barone, V. *Theor. Chem. Acc.* **2000**, *104*, 265 and the references cited therein. (b) Ruiz, E.; Rodriguez-Fortea, A.; Cano, J.; Alvarez, S. *J. Phys. Chem. Solids* **2004**, *65*, 799.

(15) (a) Chartier, A.; D'Arco, P.; Dovesi, R.; Saunders, V. R. *Phys. Rev. B* **1999**, *60*, 14042 and the references cited therein. (b) Dai, D.; Whangbo, M.-H.; Koo, H.-J.; Rocquefelte, X.; Jobic, S.; Villesuzanne, A. *Inorg. Chem.* **2005**, *44*, 2407.

(16) (a) Noodleman, L. *J. Chem. Phys.* **1981**, *74*, 5737. (b) Dai, D.; Whangbo, M.-H. *J. Chem. Phys.* **2001**, *114*, 2887. (c) Dai, D.; Whangbo, M.-H. *J. Chem. Phys.* **2003**, *118*, 29.

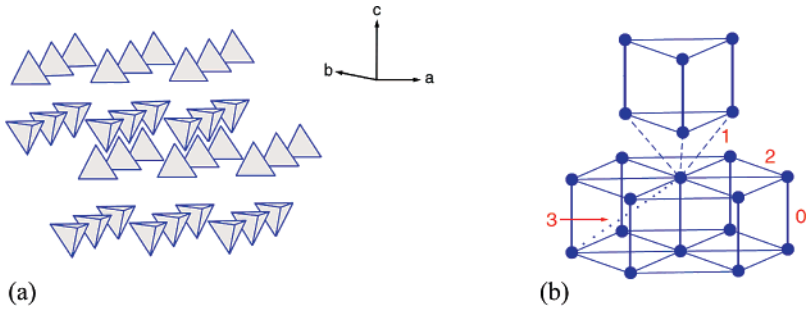

Figure 1. Schematic representations of the 3D arrangements of (a) the $(MO_4)^{3-}$ tetrahedra and (b) the M^{5+} ions in $Ba_3M_2O_8$ (M = Cr, Mn). The $(MO_4)^{3-}$ tetrahedra are shown as polyhedra in (a), and the M^{5+} ions as filled circles, in (b). The numbers 0−3 in (b) represent the spin exchange paths J_0−J_3, respectively.

where $\Delta e_{\mu\mu}$ is the energy split that results when two magnetic orbitals ϕ_μ ($\mu = 1-5$) on adjacent spin sites interact and the prefactor of the summation is related to the number of unpaired spins. There is one electron to fill the e_g level of Cr^{5+} and two electrons to fill the t_{2g} level of Fe^{4+}. If we assume that the degenerate orbitals of the e_g or t_{2g} level have an equal chance of being occupied, the $<(\Delta e)^2>$ term is approximated by[9,12]

$$Cr^{5+}\ (d^1): \quad <(\Delta e)^2> \approx \left[\left(\frac{1}{2}\right)^2 \sum_{\mu=1}^{2} (\Delta e_{\mu\mu})^2\right] \tag{4}$$

$$Fe^{4+}\ (d^4): \quad <(\Delta e)^2> \approx \frac{1}{4^2}\left[\sum_{\mu=1}^{2} (\Delta e_{\mu\mu})^2 + \left(\frac{2}{3}\right)^2 \sum_{\mu=3}^{5} (\Delta e_{\mu\mu})^2\right] \tag{5}$$

In this work, the $\Delta e_{\mu\mu}$ values for various spin dimers are evaluated by performing EHTB calculations.[18] For a variety of magnetic solids of transition metal ions it has been found[9] that their magnetic properties are well described by the $<(\Delta e)^2>$ values obtained from EHTB calculations, when both the d orbitals of the transition metal ions and the s/p orbitals of its surrounding ligands are represented by double-ζ Slater type orbitals (DZ-STO's).[19] Our calculations are carried out using the atomic parameters summarized in the Table S1 of the Supporting Information. The radial part of a DZ-STO is expressed as r^{n-1} [$c_1 \exp(-\zeta_1 r) + c_2 \exp(-\zeta_2 r)$], where n is the principal quantum number and the exponents ζ_1 and ζ_2 describe contracted and diffuse STO's, respectively (i.e., $\zeta_1 > \zeta_2$). The diffuse STO provides an orbital tail that enhances overlap between O atoms in the O···O contacts of the M−O···O−M super-superexchange paths. The $\Delta e_{\mu\mu}$ values are affected most sensitively by the exponent ζ_2 of the diffuse O 2p orbital. The ζ_2 values taken from results of electronic structure calculations for neutral atoms[19] may not be diffuse enough to describe O^{2-} ions. To make the O 2p orbital more diffuse, the ζ_2 value should be reduced. To assess how the diffuseness of the O 2p orbital affects the relative strengths of the super-superexchange interactions between adjacent

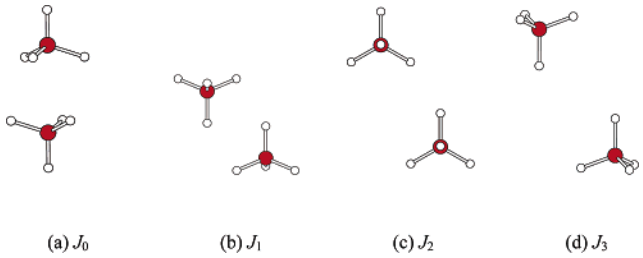

Figure 2. Spin dimers associated with the spin exchange paths J_0, J_1, J_2, and J_3 of $Ba_3M_2O_8$ (M = Cr, Mn), where the atoms M and O are represented by red and white circles, respectively.

MO_4 teterahedra, we replace ζ_2 with $(1 - x)\zeta_2$ and calculate the $<(\Delta e)^2>$ values for three values of x, i.e., 0.00, 0.05, and 0.10.

3. Results and Discussion

3.1. $Ba_3Cr_2O_8$ and $Ba_3Mn_2O_8$. $Ba_3Cr_2O_8$ is isostructural with $Ba_3Mn_2O_8$.[4,5d] The 3D arrangement of the $(MO_4)^{3-}$ tetrahedra in $Ba_3M_2O_8$ (M = Cr, Mn) is shown in Figure 1a, and that of the M^{5+} ions, in Figure 1b. The spin dimers associated with the four spin exchange paths, i.e., J_0, J_1, J_2, and J_3, are presented in Figure 2, where J_0 is the intradimer exchange interaction and J_1, J_2, and J_3 are interdimer interactions. Each spin site leads to one J_0 intradimer and $3J_1 + 6J_2 + 3J_3$ ($\equiv J'$) interdimer interactions. Magnetic susceptibility and magnetization measurements show that $Ba_3Cr_2O_8$ has a larger spin gap than does $Ba_3Mn_2O_8$ (i.e., $\Delta/k_B = 16.1$ vs 11.2 K).[4,5a−c] The magnetic susceptibilities of both $Ba_3Cr_2O_8$ and $Ba_3Mn_2O_8$ are described by a weakly interacting AFM dimer model.[4,5a−c] The J_0/k_B and J'/k_B values are respectively estimated to be −25.0 and −7.7 K for $Ba_3Cr_2O_8$[4] and −17.4 and −24.9 K for $Ba_3Mn_2O_8$.[5a−c] Thus, the intradimer exchange J_0 is stronger in $Ba_3Cr_2O_8$ than in $Ba_3Mn_2O_8$, and with respect to the intradimer exchange interaction, the interdimer interaction is much weaker in $Ba_3Cr_2O_8$ than in $Ba_3Mn_2O_8$ (i.e., $J'/J_0 = 0.3$ vs 1.4).

The $<(\Delta e)^2>$ values calculated for $Ba_3Mn_2O_8$ (Table 1) show that the exchange interaction J_0 is the dominant interaction regardless of the x value, in support of a weakly interacting spin dimer model found for $Ba_3Mn_2O_8$.[5a−c] In terms of the $<(\Delta e)^2>$ values, the J'/J_0 ratio is estimated to be slightly smaller than the experimental value (i.e., 0.84 vs 1.4). The $<(\Delta e)^2>$ values calculated for $Ba_3Cr_2O_8$ are listed in Table 2a, which reveals that the relative strengths of J_0 and J_1 depend on the value of x. With increasing x, J_0

(17) (a) Hay, P. J.; Thibeault, J. C.; Hoffmann, R. *J. Am. Chem. Soc.* **1975**, *97*, 4884. (b) Kahn, O.; Briat, B. *J. Chem. Soc., Faraday Trans. 2* **1976**, *72*, 268.
(18) Our calculations were carried out by employing the SAMOA (Structure and Molecular Orbital Analyzer) program package (Dai, D.; Ren, J.; Liang, W.; Whangbo, M.-H. http://chvamw.chem.ncsu.edu/, 2002).
(19) Clementi, E.; Roetti, C. *At. Data Nucl. Data Tables* **1974**, *14*, 177.

Table 1. Values of the Mn···Mn Distance and $<(\Delta e)^2>$ Associated with the Spin Paths J_0-J_3 in $Ba_3Mn_2O_8$[a]

path	Mn···Mn	$x = 0.10$	$x = 0.05$	$x = 0.00$
J_0	3.985	4000 (1.00)	1800 (1.00)	760 (1.00)
J_1	4.569	480 (0.12)	200 (0.11)	80 (0.10)
J_2	5.711	330 (0.08)	160 (0.09)	80 (0.10)
J_3	6.964	0 (0.00)	0 (0.00)	0 (0.00)

[a] The numbers in parentheses refer to relative strengths. The distances are in units of Å, and the $<(\Delta e)^2>$ values, in units of $(meV)^2$.

Table 2. Values of the Cr···Cr Distance, $<(\Delta e)^2>$, and $<(\Delta e)^2>_{OO}$ Associated with the Spin Paths J_0-J_3 in $Ba_3Cr_2O_8$[a]

path	Cr···Cr	$x = 0.10$	$x = 0.05$	$x = 0.00$
		(a) $<(\Delta e)^2>$		
J_0	3.937	1900 (1.00)	650 (1.00)	190 (0.90)
J_1	4.597	820 (0.44)	410 (0.62)	210 (1.00)
J_2	5.739	470 (0.25)	220 (0.34)	100 (0.50)
J_3	6.960	0 (0.00)	0 (0.00)	0 (0.00)
		(b) $<(\Delta e)^2>_{OO}$		
J_0	3.937	3700	1300	370

[a] The numbers in parentheses refer to relative strengths. The distances are in units of Å, and the $<(\Delta e)^2>$ and $<(\Delta e)^2>_{OO}$ values, in units of $(meV)^2$.

becomes stronger while J_1 and J_2 become weaker such that J_0 is the dominant exchange interaction for $x = 0.05$ and 0.10. However, the J'/J_0 ratio for $Ba_3Cr_2O_8$ estimated in terms of $<(\Delta e)^2>$ is unreasonably large compared with the experimental value (i.e., 2.8 for $x = 0.10$ vs 0.3) and is greater than that for $Ba_3Mn_2O_8$ in disagreement with experiment (i.e., 2.8/0.84 vs 0.3/1.4). Furthermore, the $<(\Delta e)^2>$ value for the exchange path J_0 is much smaller for $Ba_3Cr_2O_8$ than for $Ba_3Mn_2O_8$ [i.e., 1900 vs 4000 $(meV)^2$ for $x = 1.0$] although the experimental J_0 value is greater in magnitude for $Ba_3Cr_2O_8$ than for $Ba_3Mn_2O_8$ (i.e., $J_0/k_B = -25.0$ vs -17.4 K).

The aforementioned discrepancies associated with the $<(\Delta e)^2>$ values of $Ba_3Cr_2O_8$ make us to doubt the validity of the assumption leading to eq 4, namely, the degenerate orbitals ϕ_1 and ϕ_2 representing the e_g level have an equal chance of being occupied. Therefore, we consider the occurrence of orbital ordering in $Ba_3Cr_2O_8$, i.e., the occupation of only one of the two orbitals ϕ_1 and ϕ_2. Then, the $<(\Delta e)^2>$ value in this case, which will be referred to as $<(\Delta e)^2>_{OO}$, is approximated by

$$Cr^{5+}\ (d^1): \quad <(\Delta e)^2>_{OO} \approx (\Delta e_{11})^2 \qquad (6)$$

where it is assumed, without loss of generality, that ϕ_1 is occupied but ϕ_2 is not. The orbital ordering should be dictated by the exchange path leading to the strongest exchange interaction (i.e., J_0 in the present case, which is reproduced by $x = 0.05$ and 0.10). As shown in Table 2b, the $<(\Delta e)^2>_{OO}$ values calculated for the exchange path J_0 of $Ba_3Cr_2O_8$ are now comparable in magnitude to the corresponding $<(\Delta e)^2>$ values of $Ba_3Mn_2O_8$. The effective on-site repulsion U_{eff} is expected to be greater for the Mn^{5+} ion than for the Cr^{5+} ion. Thus, it is understandable that the J_0 value is slightly greater in magnitude for $Ba_3Cr_2O_8$ than for $Ba_3Mn_2O_8$ ($J_0/k_B = -25.0$ vs -17.4 K). When one e_g orbital (i.e., ϕ_1) is preferentially occupied, their interactions lead to the bonding and antibonding combinations leading to the Δe_{11} value, as depicted in Figure 3. Once the shape and orientation of the magnetic orbital are fixed in space by the intradimer exchange interaction, the interdimer exchange interactions between such magnetic orbitals become weak. This provides a natural explanation for why the J'/J_0 value of $Ba_3Cr_2O_8$ is much smaller than that of $Ba_3Mn_2O_8$.

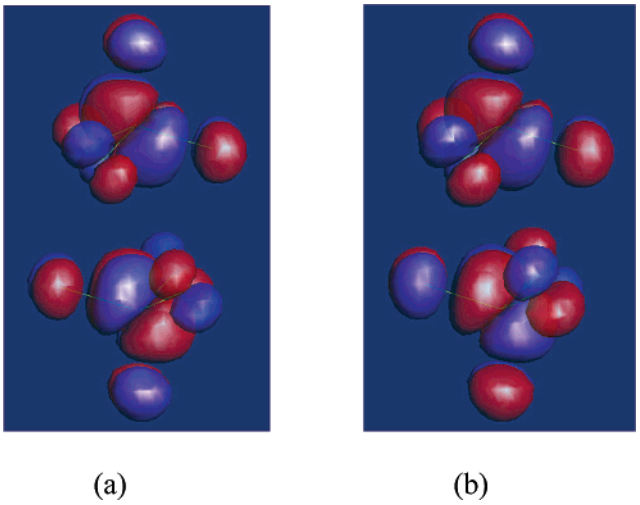

Figure 3. (a) Bonding and (b) antibonding combinations of one e_g orbital (e.g., ϕ_1) of $Ba_3Cr_2O_8$ leading to the Δe_{11} value.

B. Na_4FeO_4. The existence of Na_4FeO_4 was reported half a century ago,[7c] but its crystal structure was determined only recently.[7a,b] According to ^{57}Fe Mössbauer effect data, the Fe^{4+} (d^4) ions of Na_4FeO_4 are in high-spin state.[7a] The magnetic susceptibility of Na_4FeO_4 follows a Curie−Weiss behavior with the Weiss constant $\Theta \approx -37$ K and shows a 3D AFM ordering below $T_N = 16$ K.[7a] The powder neutron diffraction measurements at 2 K show a magnetic superstructure (0.0, 0.5, 0.0).[7a] The 3D arrangement of $(FeO_4)^{4-}$ tetrahedra in Na_4FeO_4 is depicted in Figure 4a, and that of the Fe^{4+} ions, in Figure 4b. According to the $<(\Delta e)^2>$ values calculated for the spin exchange paths J_1-J_9 of Na_4FeO_4 (Table 3), there is no dominant spin exchange interaction. Nevertheless, it is clear for $x = 0.05$ and 0.10 that five spin exchange interactions (i.e., J_1, J_2, J_5, J_6, and J_9) are substantially stronger than the remaining four spin exchange interactions (i.e., J_3, J_4, J_7, and J_8). As shown in Figure 5, the four spin exchange interactions J_2, J_5, J_6, and J_9 lead to the 3D AFM arrangement of spins with a (0.0, 0.5, 0.0) superstructure. This explains the magnetic superstructure of Na_4FeO_4 observed at 2 K.[7a] In this superstructure, the spin exchange interactions J_1, J_3, J_4, J_7, and J_8 are frustrated. However, these interactions are weak, and their frustration is expected since they are the second-nearest-neighbor interactions of antiferromagnetic "square" lattices. Furthermore, the $|\Theta|/T_N$ value of 2.3 is low. Though somewhat arbitrary, the condition $|\Theta|/T_N > 10$ is taken as a criterion for the presence of geometric spin frustration.[20,21] Consequently, Na_4FeO_4 should not be considered to possess geometric spin frustration.

Each Fe^{4+} ion has only two electrons to fill the degenerate t_{2g} level. Thus, in principle, it is necessary to consider possible orbital ordering in Na_4FeO_4. However, since there is no dominant spin exchange interaction, orbital ordering

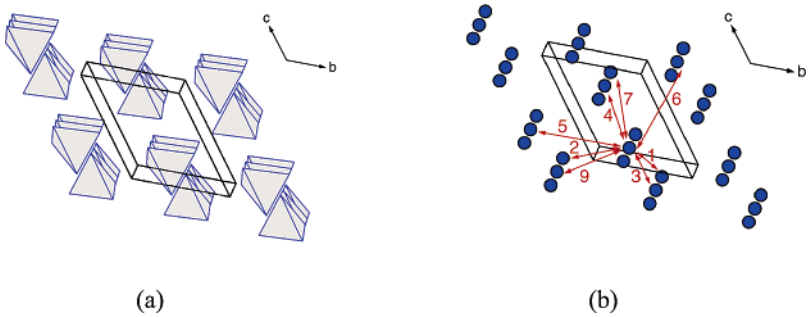

Figure 4. Schematic representations of the 3D arrangements of (a) the $(FeO_4)^{4-}$ tetrahedra and (b) the Fe^{4+} ions in Na_4FeO_4. The $(FeO_4)^{4-}$ tetrahedra are shown as polyhedra in (a), and the Fe^{4+} ions, as filled circles in (b). The numbers 1−9 in (b) represent the spin exchange paths J_1−J_9, respectively.

Table 3. Values of the Fe···Fe Distance and $<(\Delta e)^2>$ Associated with the Spin Paths J_1−J_9 in Na_4FeO_4[a]

path	Fe···Fe	$x = 0.10$	$x = 0.05$	$x = 0.00$
J_1	4.816	52 (0.66)	22 (0.47)	11 (0.30)
J_2	4.091	51 (0.65)	47 (1.00)	37 (1.00)
J_3	5.121	17 (0.22)	7 (0.15)	4 (0.11)
J_4	5.263	11 (0.14)	11 (0.23)	9 (0.24)
J_5	5.768	79 (1.00)	27 (0.57)	9 (0.24)
J_6	5.769	60 (0.76)	20 (0.43)	7 (0.19)
J_7	6.465	40 (0.51)	13 (0.28)	4 (0.11)
J_8	6.562	40 (0.51)	14 (0.30)	4 (0.11)
J_9	6.855	51 (0.65)	19 (0.40)	7 (0.19)

[a] The numbers in parentheses refer to relative strengths. The distances are in units of Å, and the $<(\Delta e)^2>$ values, in units of $(meV)^2$.

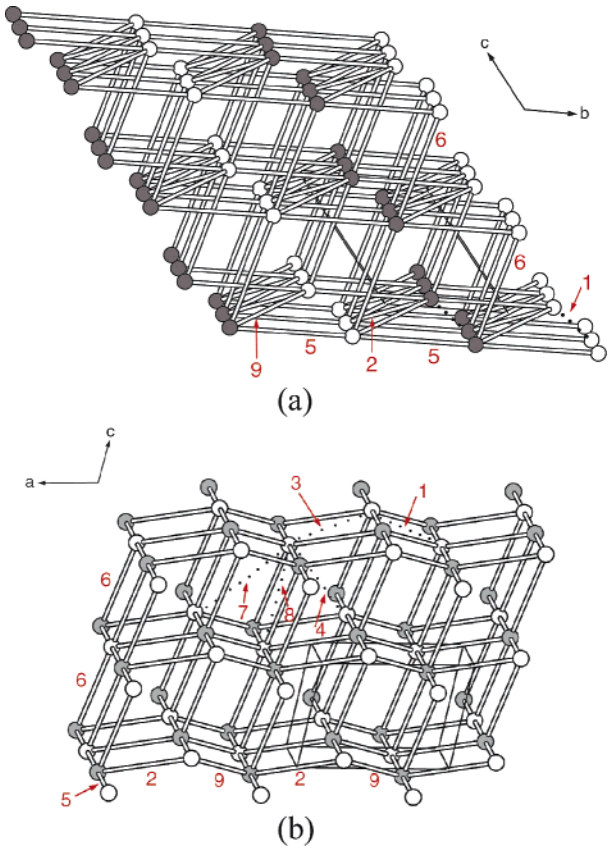

Figure 5. Two perspective views of the 3D AFM spin lattice of Na_4FeO_4 made up of the spin exchange paths J_2, J_5, J_6, and J_9, where the filled and open circles represent up-spin and down-spin sites, respectively. The spin exchange interactions J_1, J_3, J_4, J_7, and J_8 lead to magnetic frustration.

is not expected to occur. Thus, the $<(\Delta e)^2>$ values should describe the relative strengths of J_1−J_9 reasonably well. This is the case in view of the fact that the observed magnetic superstructure is explained by the $<(\Delta e)^2>$ values.

C. Ba_2CoO_4. Boulahya et al.[8a] reported that the magnetic susceptibility of Ba_2CoO_4 follows a Curie−Weiss behavior in the range from 100 to 300 K with the Weiss constant $\Theta = -116$ K and shows a 3D AFM ordering below $T_N = 23$ K. Their powder neutron diffraction study at 4 K reveals a magnetic superstructure (0.5, 0.0, 0.5). Independently, Jin et al.[8b] found essentially the same results, i.e., the Curie−Weiss behavior in the range from ~150 to 350 K, $\Theta \approx -110$ K and $T_N = 25$ K. It has been suggested[8a,b] that the finding for $T_N \ll |\Theta|$ results either from reduced dimensionality of magnetic interactions or from possible magnetic frustration in Ba_2CoO_4.

The 3D arrangement of $(CoO_4)^{4-}$ tetrahedra in Ba_2CoO_4 is shown in Figure 6a, and that of the corresponding Co^{4+} ions, in Figure 6b. The $<(\Delta e)^2>$ values calculated for the spin exchange paths J_1−J_8 of Ba_2CoO_4 are presented in Table 4. Although there is no dominant spin exchange interaction, it is clear for $x = 0.05$ and 0.10 that four spin exchange interactions (i.e., J_1, J_3, J_6, and J_7) are substantially stronger than the remaining four spin exchange interactions (i.e., J_2, J_4, J_5, and J_8). As depicted in Figure 7a, the two strong spin exchange interactions J_1 and J_3 form chains along the *b*-direction, and these chains can be antiferromagnetically arranged along the *a*-direction because the spin exchange J_7 is much stronger than the spin exchanges J_2 and J_5. Thus, the three strong interactions J_1, J_3, and J_7 form a layer, and these layers interact antiferromagnetically through the strong exchange J_6 (Figure 7b). As a consequence, Ba_2CoO_4 is predicted to have a (0.5, 0.0, 0.5) superstructure as shown in Figure 7c, in agreement with the magnetic superstructure of Ba_2CoO_4 at 4 K.[8a] As described above, the magnetic interactions leading to the (0.5, 0.0, 0.5) superstructure are 3D in nature. In this superstructure, the "intralayer" spin exchange interactions J_2 and J_5 are frustrated in a distorted triangular lattice, and so is the "interlayer" spin exchange interaction J_8. The presence of such magnetic frustration explains why $T_N \ll |\Theta|$ in Ba_2CoO_4, as anticipated,[8a,b] although the $|\Theta|/T_N$ value of 4.4 is well below 10, beyond which geometric spin frustration is commonly regarded to exist.[20,21]

(20) Greedan, J. E. *J. Mater. Chem.* **2001**, *11*, 37.
(21) Schiffer, P.; Ramirez, A. P. *Commun. Condens. Matter Phys.* **1996**, *10*, 21.

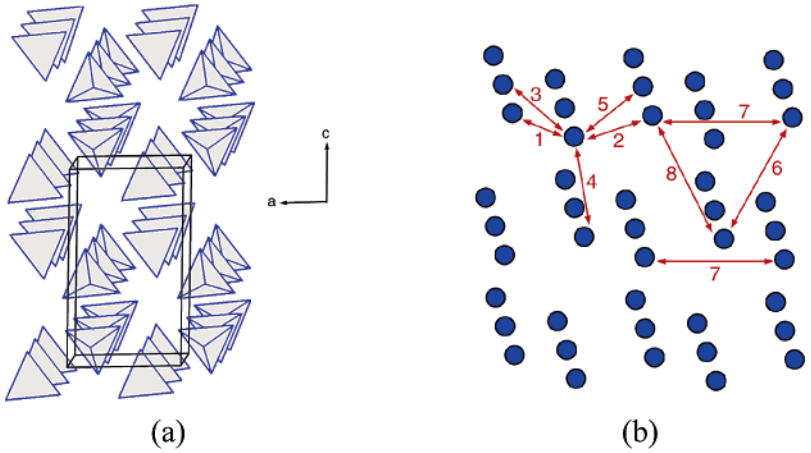

Figure 6. Schematic representations of the 3D arrangements of (a) the $(CoO_4)^{4-}$ tetrahedra and (b) the Co^{4+} ions in Ba_2CoO_4. The $(CoO_4)^{4-}$ tetrahedra are shown as polyhedra in (a), and the Co^{4+} ions, as filled circles in (b). The numbers 1−8 in (b) represent the spin exchange paths J_1−J_8, respectively.

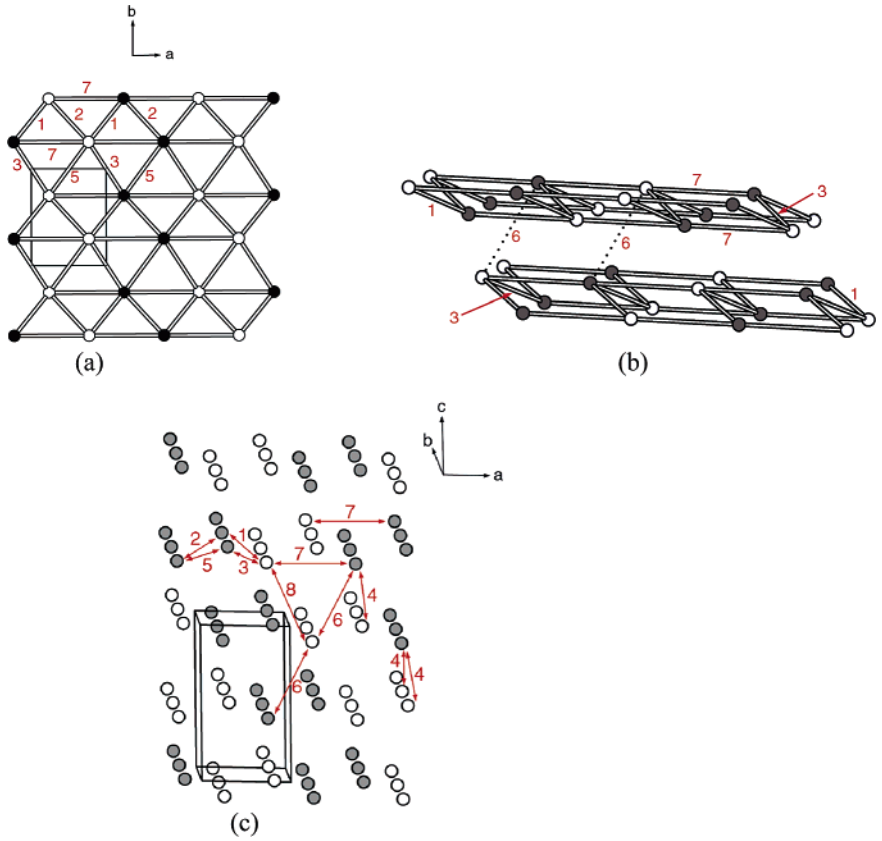

Figure 7. Spin lattice of Ba_2CoO_4: (a) a layer made up of the spin exchange paths J_1, J_3 and J_7; (b) two layers made up of J_1, J_3, and J_7 interacting antiferromagnetically through the spin exchange J_6; (c) 3D AFM lattice made up of J_1, J_3, J_6, and J_7. The filled and open circles represent up-spin and down-spin sites, respectively. The "intralayer" spin exchange interactions J_2 and J_5 are frustrated, and so is the "interlayer" spin exchange interaction J_8.

4. Concluding Remarks

Although the magnetic oxides $Ba_3Cr_2O_8$, $Ba_3Mn_2O_8$, Na_4FeO_4, and Ba_2CoO_4 have a network of isolated MO_4 (M = Cr, Mn, Fe, Co) tetrahedra well-separated from each other, the super-superexchange interactions between adjacent MO_4 tetrahedra are substantial and determine the magnetic structures of these oxides. In good agreement with experiment, our spin dimer analysis predicts a weakly interacting isolated AFM dimer model for $Ba_3Mn_2O_8$, the (0.0, 0.5, 0.0) magnetic superstructure for Na_4FeO_4, and the (0.5, 0.0, 0.5) magnetic superstructure for Ba_2CoO_4. The magnetic interactions of

Table 4. Values of the Co···Co Distance and $<(\Delta e)^2>$ Values Associated with the Spin Paths J_1−J_8 in Ba_2CoO_4[a]

path	Co···Co	$x = 0.10$	$x = 0.05$	$x = 0.00$
J_1	4.653	270 (0.82)	200 (1.00)	84 (1.00)
J_2	4.825	47 (0.14)	34 (0.17)	36 (0.43)
J_3	5.280	160 (0.49)	75 (0.38)	22 (0.26)
J_4	5.289	110 (0.35)	48 (0.24)	20 (0.24)
J_5	5.433	130 (0.39)	62 (0.32)	25 (0.30)
J_6	5.889	160 (0.48)	48 (0.24)	14 (0.17)
J_7	5.891	330 (1.00)	130 (0.66)	50 (0.60)
J_8	6.059	81 (0.25)	30 (0.15)	7 (0.08)

[a] The numbers in parentheses refer to relative strengths. The distances are in units of Å, and the $<(\Delta e)^2>$ values in units of $(meV)^2$.

both Na_4FeO_4 and Ba_2CoO_4 are 3D in nature, and the reasonably large value of $|\Theta|/T_N$ in Ba_2CoO_4 is consistent with the presence of some geometric spin frustration. Our analysis also predicts a weakly interacting isolated AFM dimer model for $Ba_3Cr_2O_8$. However, the comparison of the intra- and interdimer spin exchange interactions of $Ba_3Cr_2O_8$ and $Ba_3Mn_2O_8$ indicates that orbital ordering should be present in $Ba_3Cr_2O_8$. This study demonstrates that our spin dimer analysis, though qualitative, can be employed to correctly interpret experimental magnetic data.

Acknowledgment. This research was supported by the Office of Basic Energy Sciences, Division of Materials Sciences, U.S. Department of Energy, under Grant DE-FG02-86ER45259, and by the Kyung Hee University Research Fund in 2006 (Grant KHU-20060347).

Supporting Information Available: Table S1, listing the atomic parameters employed for the EHTB calculations. This material is available free of charge via the Internet at http://pubs.acs.org.

IC061773C